Threshold memristor-based inverse radial basis neuron for motion detection

Zuheng Wu(吴祖恒), Mengjie Jiang(姜梦婕), Ying Yang(杨颖), Zihao Wang(王子昊), Wenbin Guo(郭文斌), Jianxun Zou(邹建勋), Zhe Feng(冯哲), Yunlai Zhu(朱云来), Chen Luo(骆晨), Yuehua Dai(代月花)
Citation: Chin. Phys. B. 35, 108401 (2026). DOI: 10.1088/1674-1056/ae1fe5 | CSTR: 32038.14.CPB.ae1fe5
http://cpb.iphy.ac.cn; http://iopscience.iop.org/cpb

What follows is a list of articles you may be interested in

One memristor–one electrolyte-gated transistor-based high energy-efficient dropout neuronal units

Yalin Li(李亚霖), Kailu Shi(时凯璐), Yixin Zhu(朱一新), Xiao Fang(方晓), Hangyuan Cui(崔航源), Qing Wan(万青), Changjin Wan(万昌锦)
Chin. Phys. B. 33, 068401 (2024). DOI: 10.1088/1674-1056/ad39d6

Memristor's characteristics: From non-ideal to ideal

Fan Sun(孙帆), Jing Su(粟静), Jie Li(李杰), Shukai Duan(段书凯), Xiaofang Hu(胡小方)
Chin. Phys. B. 32, 028401 (2023). DOI: 10.1088/1674-1056/ac7548

A review on the design of ternary logic circuits

Xiao-Yuan Wang(王晓媛), Chuan-Tao Dong(董传涛), Zhi-Ru Wu(吴志茹), Zhi-Qun Cheng(程知群)
Chin. Phys. B. 30, 128402 (2021). DOI: 10.1088/1674-1056/ac248b

Artificial synaptic behavior of the SBT-memristor

Gang Dou(窦刚), Ming-Long Dou(窦明龙), Ren-Yuan Liu(刘任远), Mei Guo(郭梅)
Chin. Phys. B. 30, 078401 (2021). DOI: 10.1088/1674-1056/ac05a3

SBT-memristor-based crossbar memory circuit

Mei Guo(郭梅), Ren-Yuan Liu(刘任远), Ming-Long Dou(窦明龙), Gang Dou(窦刚)
Chin. Phys. B. 30, 068402 (2021). DOI: 10.1088/1674-1056/abd7dc

---

Threshold memristor-based inverse radial basis neuron for motion detection

Zuheng Wu(吴祖恒)[1], Mengjie Jiang(姜梦婕)[1], Ying Yang(杨颖)[1], Zihao Wang(王子昊)[1], Wenbin Guo(郭文斌)[1], Jianxun Zou(邹建勋)[1], Zhe Feng(冯哲)[1,†], Yunlai Zhu(朱云来)[1], Chen Luo(骆晨)[2,‡], and Yuehua Dai(代月花)[1]

[1] *School of Integrated Circuits, Anhui University, Hefei* 230601, *China*

[2] *Jiangsu Province Engineering Research Center of Integrated Circuit Reliability Technology and Testing System, School of Integrated Circuit Science and Engineering, Wuxi University, Wuxi* 214105, *China*

(Received 12 September 2025; revised manuscript received 11 November 2025; accepted manuscript online 17 November 2025)

Visual motion detection plays a crucial role in computer vision applications including human behavior understanding and traffic monitoring. Traditional motion detection methods lack the selective response mechanism of biological visual neurons and cannot effectively distinguish between moving objects and background information. This paper proposes an inverse radial basis neuron (IRBN) circuit based on a threshold-switched memristor that realizes "near-suppression far-enhancement" response characteristics opposite to conventional radial basis functions. The voltage–frequency responses of IRBN can be modulated through adjustment of the memristor dielectric constant and circuit parameters. Application of IRBN characteristics to gait energy image (GEI) processing achieves suppression of low-grayscale background regions and enhancement of high-grayscale motion silhouettes with an edge preservation index of 9.466, which is 2 to 30 times higher than traditional image processing methods. This work provides a new implementation approach for biomimetic motion vision detection.

Keywords: threshold switching, memristor, inverse radial basis neuron (IRBN) circuit

PACS: 84.35.+q, 73.40.Sx, 07.05.Mh, 87.18.Sn

DOI: 10.1088/1674-1056/ae1fe5 **CSTR:** 32038.14.CPB.ae1fe5

1. Introduction

Visual motion detection is one of the core technologies in computer vision, playing a crucial role in applications such as human behavior understanding, traffic monitoring, industrial automation, and ecological protection.[1] However, traditional motion detection methods mainly include frame difference, background subtraction, and optical flow methods.[2] Frame difference identifies regions where pixel values change by comparing consecutive video frames.[3] Background subtraction detects foreground moving targets by establishing background models.[4] Optical flow analyzes motion patterns by calculating motion vectors of pixels in image sequences.[5] Nevertheless, these methods primarily rely on pixel-level numerical calculations and lack the selective response mechanisms of biological visual neurons.[6] More importantly, these methods cannot effectively distinguish between moving objects and background information, failing to suppress weak signals while enhancing strong signals. Consequently, in complex dynamic scenes, not only does detection accuracy decrease, but computational energy consumption remains high.[7]

By contrast, biological vision has evolved over long periods to achieve highly efficient motion detection. In bright conditions, the retina's cone cells handle color perception and central fine vision, while rod cells in dim light manage peripheral low-light motion detection.[8,9] Neuronal ganglion cells (RGCs) in the retinal inner layer transmit information to the brain, with motion-sensitive subpopulations directly perceiving object displacement and encoding direction and velocity.[10] Hence, translating these biological principles into electronic systems is beneficial for developing high-efficiency motion detection systems.

In recent years, memristors as the fourth fundamental circuit element have attracted widespread attention for developing bio-inspired electronic systems. Memristors possess unique resistance memory characteristics and threshold switching behavior, providing an ideal hardware foundation for neuromorphic computing. Compared to traditional electronic components, memristors can better simulate biological synapses and neuronal functions while offering advantages of simple structure,[11] low power consumption,[12] and high integration density.[13] Particularly, threshold switching (TS) memristors switch from high resistance state (HRS) to low resistance state (LRS) when input voltage exceeds the threshold,

†Corresponding author. E-mail: zack@ahu.edu.cn

‡Corresponding author. E-mail: chen_luo@fudan.edu.cn

© 2026 Chinese Physical Society and IOP Publishing Ltd. All rights, including for text and data mining, AI training, and similar technologies, are reserved.

making this switching characteristic suitable for implementing neuronal firing behavior.[14,15]

Meanwhile, the leaky integrate-and-fire (LIF) neuron model has been widely adopted for its ability to effectively capture basic characteristics of biological neurons. Existing research indicates that radial basis function (RBF) based neurons can be successfully implemented through the LIF model.[16] RBF neural networks possess nonlinear mapping capabilities and local synaptic plasticity with relatively simple network structures.[17] However, traditional RBF neurons exhibit "near-enhancement far-suppression" activation patterns, producing strong responses to inputs near the center while generating weak responses to inputs far from the center.[18] This characteristic shows significant limitations in motion detection applications, unable to achieve effective background noise suppression and selective enhancement of moving targets.

In this work, an inverse radial basis neuron (IRBN) circuit is designed for motion detection applications. In contrast to RBF neurons, the IRBN exhibits a "near-suppression far-enhancement" response characteristic, effectively suppressing low-intensity input signals while enhancing high-intensity input signals. This design principle aligns closely with the visual mismatch negativity (vMMN) phenomenon observed in biological visual systems. The vMMN, as a specific component of event-related potentials, reflects the brain's automatic detection mechanism for visual stimulus prediction errors.[19] The Poole–Frenkel conduction mechanism based memristor is used to construct the IRBN circuit. Through the combination of input conversion modules and oscillating neurons, the "near-suppression far-enhancement" voltage–frequency (V–F) response characteristics are achieved. The input conversion module includes an absolute value unit, an inverting amplifier, a subtractor, and an auxiliary bias voltage, while oscillating neurons consist of a TS memristor, a capacitor, and a resistor. By adjusting the memristor's dielectric constant, switching windows and response boundaries can be modulated. Furthermore, by modifying circuit parameters such as series resistance and amplification factors, the output frequency range can be tuned while maintaining a constant minimum output frequency. We further mapped the IRBN circuit characteristics into an image processing algorithm and applied it to gait energy image (GEI) analysis. GEI recognition is a typical motion pattern detection and classification task. Specifically, GEI[20] compresses temporal motion information into a spatial feature representation by superimposing silhouette sequences within a complete gait cycle. Within GEI, static background regions exhibit low grey values due to minimal pixel variation, whereas human silhouette regions containing motion information display high grey values. Experimental results demonstrate that the IRBN method achieves suppression of low-grayscale background regions and enhancement of high-grayscale motion silhouettes, with an edge preservation index reaching 9.466, which is 2 to 30 times higher than traditional image processing methods, providing a new implementation approach for biomimetic motion vision detection.

2. The biological mechanism of motion detection

As illustrated in Fig. 1, the retina contains rod and cone cells, which are photoreceptors that detect light and convert it into neural signals. RGCs are located in the inner layer of the retina, and their axons form the optic nerve, which transmits processed visual information to the brain. Cone cells function best in bright light and are responsible for color vision and high-resolution vision, and are more sensitive for detailed detection of moving objects in central vision. Rod cells are more sensitive in low-light conditions, are distributed in the retinal periphery, and are suitable for motion detection in low light, especially in peripheral vision. RGC neurons are responsible for transmitting visual information to the brain. A subset of these neurons shows increased sensitivity to motion-related information, allowing them to monitor the position of objects as they cross the retina. In addition, these cells are responsible for transmitting this information to the visual cortex. RGC neurons use motion detection to determine the direction and speed of motion.

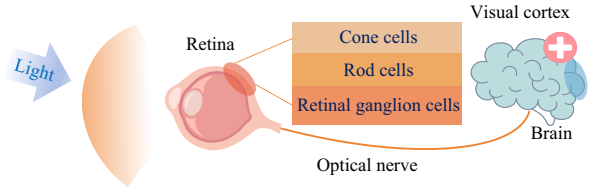

Fig. 1. Schematic diagram of biological vision systems. Biological photoreceptors convert light stimuli from moving objects into pulsed potentials. The encoded information is eventually sent to the brain for further processing.

3. The TS memristor

In this work, the circuit experiments were conducted using LTSPICE simulation. The TS memristor model is based on the Poole–Frenkel conduction mechanism.[21,22] First, Fig. 2(a) displays the I–V characteristics of the TS memristor. The device exhibits typical TS characteristics. When the input voltage sweep exceeds the threshold voltage ($V_{\rm th}$), the device switches from HRS to LRS. When the reverse scan voltage is lower than the hold voltage ($V_{\rm h}$), the device switches back from LRS to HRS. Furthermore, Fig. 2(b) further investigates the effect of the dielectric constant ($\varepsilon_{\rm r}$) on the adjustment of the switching window. As the dielectric constant increases, the switching window (the difference between $V_{\rm th}$ and

V_h) also increases. The adjustable switching window enables the adjustability of IRBN circuit response properties for meeting different application requirements.

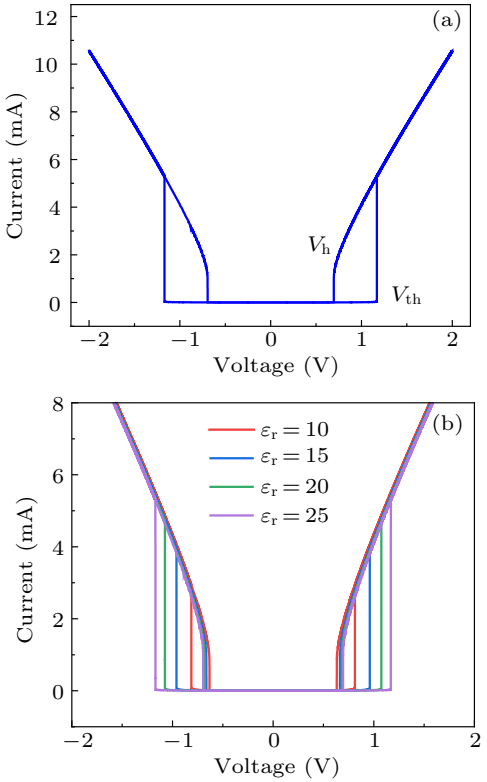

Fig. 2. (a) The typically *I*–*V* characteristics of the TS memristor model. (b) The dielectric constant influence on the device characteristics.

4. Memristor-based inverse radial basis spiking neuron circuit

To achieve motion detection in dynamic scenes,[23] we propose an IRBN circuit scheme for spike neural networks, as shown in Fig. 3.

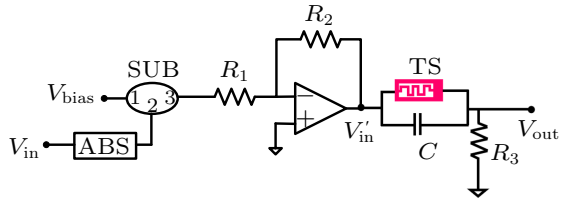

Fig. 3. The schematic diagram of the proposed IRBN circuit diagram.

The circuit structure of the IRBN consists of an input conversion module and an oscillating neuron (a TS memristor, a capacitor, and a resistor). The input conversion module comprises an absolute value unit, an inverting amplifier module, a subtractor, and an auxiliary voltage bias. The IRBN neurons have been engineered to facilitate the detection of movement. The memristor is connected in parallel with a capacitor to represent the somatic part of a biological neuron, and an inverter amplifier is used to regulate the input signal. When an input voltage signal is applied to the IRBN circuit, the absolute value unit converts the input voltage value to its absolute value. The subtractor calculates the difference between the input voltage signal and the bias voltage to obtain the differential signal. The inverting amplifier module then linearly amplifies the converted input voltage signal by a specific ratio. Finally, the output frequency of the IRBN circuit decreases and then increases, reflecting a negative trend similar to vMMN, indicating visual mismatch detection. Here, the value of the resistor R_1 is 1 kΩ and the value of R_2 is 2 kΩ. When the value of R_2 is modified, the node voltage of V'_{in} can be adjusted. Therefore, the voltages input to the node V'_{in} at different input voltages (V_{in}) follow Eq. (1):

$$V'_{in} = A\left(|V_{in}| - V_{bias}\right). \tag{1}$$

As demonstrated in Figs. 4(a) and 4(b), the output frequency characteristics of the IRBN circuit are exhibited for input voltage ranges of −0.8 V to 0 V and 0 V to 0.8 V, respectively. The simulation results indicate that the negative characteristics similar to biological visual mismatch have been successfully achieved. The circuit's amplification factor is currently set to 2 (with R_1 set to 1 kΩ and R_2 set to 2 kΩ). The results indicate that the IRBN circuits exhibit inverse radial basis function characteristics.

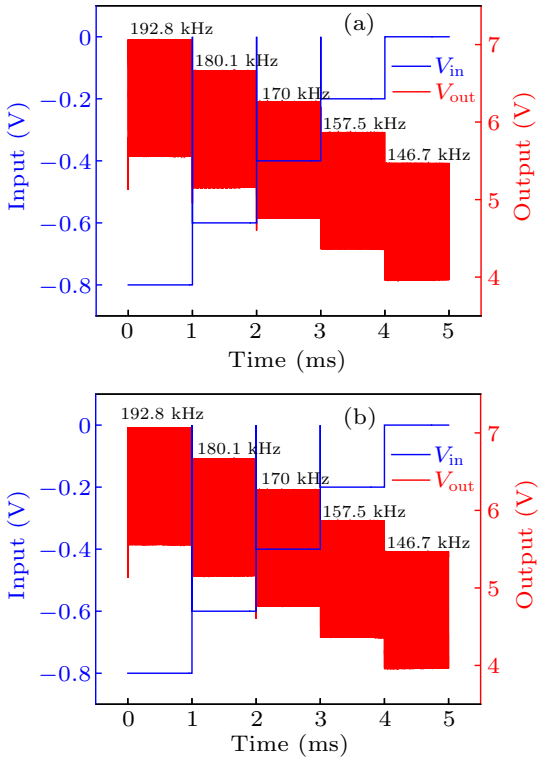

Fig. 4. The real time response of the IRBN circuit under (a) −0.8 V to 0 V and (b) 0 V to 0.8 V input voltage.

Here, the adjustability of the response characteristics of the IRBN circuit is further investigated. The circuit configuration remains consistent with that shown in Fig. 3. The boundary of the IRBN circuit response can be modified through the adjustment of the dielectric constant of the memristor model, as illustrated in Fig. 5. The findings demonstrate that when the

TS memristor model possesses distinct dielectric constants, the IRBN circuit exhibits a discernible capacity to differentiate the boundaries. Furthermore, when the dielectric constant of the TS memristor model is modified, the bias voltage of the IRBN circuit must also be modified simultaneously. This phenomenon can be attributed to the fact that as the dielectric constant of the TS memristor model decreases, its switching window also decreases, and the output frequency of the neuron circuit increases. Consequently, a simultaneous reduction of the bias voltage is required. That is, the bias voltage is determined on the basis of the minimum output frequency that has been set.

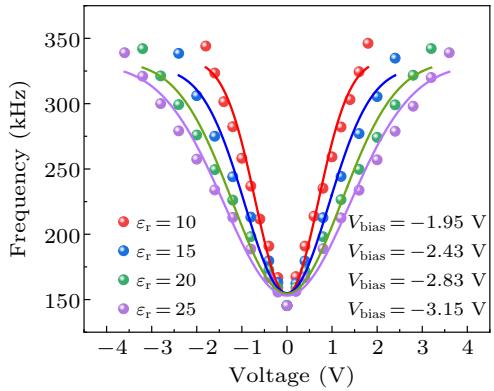

Fig. 5. The response tendency of the IRBN circuit under −4 V to 4 V input voltage pulses. The TS memristor model with different dielectric constants are used to modify the response characteristics.

Given that the coupling relationship between the dielectric constant and the bias voltage provides a "longitudinal" tuning pathway for the IRBN circuit response, we further explored whether the frequency dynamic range could be extended solely through "lateral" adjustment of internal circuit component parameters, without altering the minimum output frequency. Subsequently, we attempted to modify various parameter values within the circuit model depicted in Fig. 3, such as resistors and capacitors. Figure 6 demonstrates that parameter adjustments can alter the circuit's output frequency range while maintaining the minimum output frequency, thereby broadening its application scenarios. Figures 6(a) and 6(b) demonstrate the influence of the internal series resistor R_3 on the output characteristics: as the series resistance increases, the circuit output frequency decreases, indicating an inverse relationship between output frequency and series resistance. Figures 6(c) and Fig. 6(d) illustrate the regulatory effect of the gain in the inverting amplifier within the input conversion module on the circuit's output response. Gain variation directly alters the input voltage at node V'_{in}, whilst the circuit output frequency is proportional to the absolute value of the input voltage. Consequently, a decrease in the absolute input voltage leads to a corresponding reduction in output frequency. It is noteworthy that the minimum output frequency is determined by the magnitude of the bias voltage. Further reduction of V_{bias} can suppress the minimum output frequency to zero (as shown in Fig. 6(d)), thereby achieving full-range adjustability from zero to the target value. This enables the circuit to detect finer motion variations, significantly expanding its application prospects.

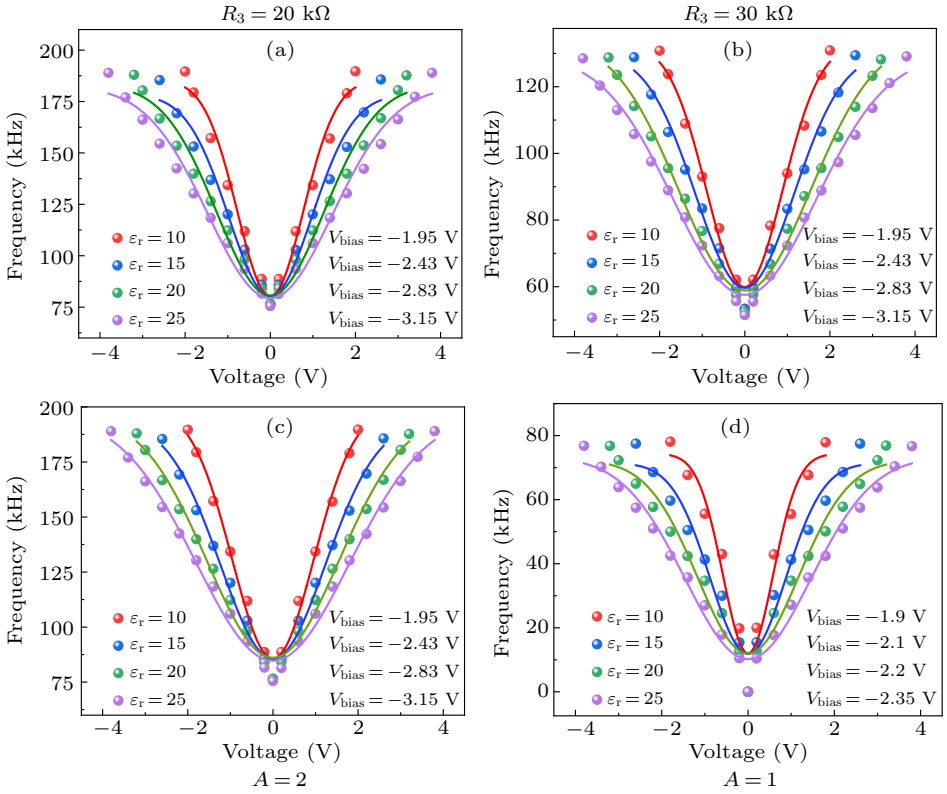

Fig. 6. Frequency characteristic curves for different output ranges obtained by changing the circuit parameters. Here, TS memristor models with different dielectric constants are used to modify the response characteristics.

Furthermore, to evaluate the dynamic response characteristics of the IRBN circuit under input swing conditions, the response characteristics of this circuit were tested within the same input range (−3 V to 3 V). As shown in Fig. 7, the output frequency characteristics of the circuit can be obtained. As illustrated in Figs. 7(a) and 7(b), increasing the series resistance leads to a corresponding increase in the time constant of the charging and discharging process. This in turn causes a significant delay in the charging and discharging process, thereby reducing the oscillation frequency. Consequently, the output frequency decreases with increasing series resistance. When the series resistance is fixed, as depicted in Figs. 7(b) and 7(c), halving the circuit's amplification gain reduces the absolute value of the input voltage at node V'_{in}, thereby lowering the output frequency. It can be verified that further reduction of V_{bias} suppresses the minimum output frequency to zero (as shown in Fig. 7(c)). Thus, through coordinated adjustment of the series resistance and input voltage, the output frequency of the IRBN circuit can be finely and continuously controlled within the same input range.

To investigate the feasibility of the IRBN circuit for motion detection application, the 'near-suppression far-enhancement' characteristics of the IRBN circuit are used to simulate the central inhibition peripheral facilitation mechanism of biological visual neurons. This mechanism forms a negative feedback loop, enabling feature selection and noise filtering capabilities. Notably, the grey-level distribution characteristics of GEI intrinsically align with the V–F response properties of IRBN. Low grey-levels correspond to low stimulation and low output frequency, while high grey-levels correspond to high stimulation and high output frequency. Therefore, through the V–F relationship of the IRBN circuit, the GEI can be directly mapped as the input to the IRBN, as shown in Figs. 8(a) and 8(b). The final frequency characteristic curve that has been selected for the gait recognition experiment corresponds to a dielectric constant of 25, as illustrated in Fig. 7(c). When the input voltage is in proximity to 0 V (corresponding to low background grey levels), the output frequency range of the IRBN circuit is compressed to a starting point that is proximate to zero frequency. As the absolute value of the input voltage increases (corresponding to high contour grey levels), the frequency rises accordingly. This approach enables full-range adjustability from 0 to the target frequency, facilitating the detection of finer grey-level changes and enhancing sensitivity to moving contours. To validate the effectiveness of this mapping relationship, we constructed an image preprocessing algorithm based on the IRBN circuit's V–F characteristic data obtained through LTSPICE simulation. This algorithm linearly maps the GEI pixel grey values to the IRBN input voltage. Then, the corresponding frequency output is interpolated using the V–F characteristic lookup table. The frequency is subsequently normalized to generate an enhanced image. As illustrated in Fig. 8(c), this mapping process causes low-grayscale background regions to fall within the IRBN suppression range, resulting in a frequency reduction. Conversely, high-grayscale contour regions fall within the enhancement range, leading to a frequency increment. This achieves selective enhancement of motion features.

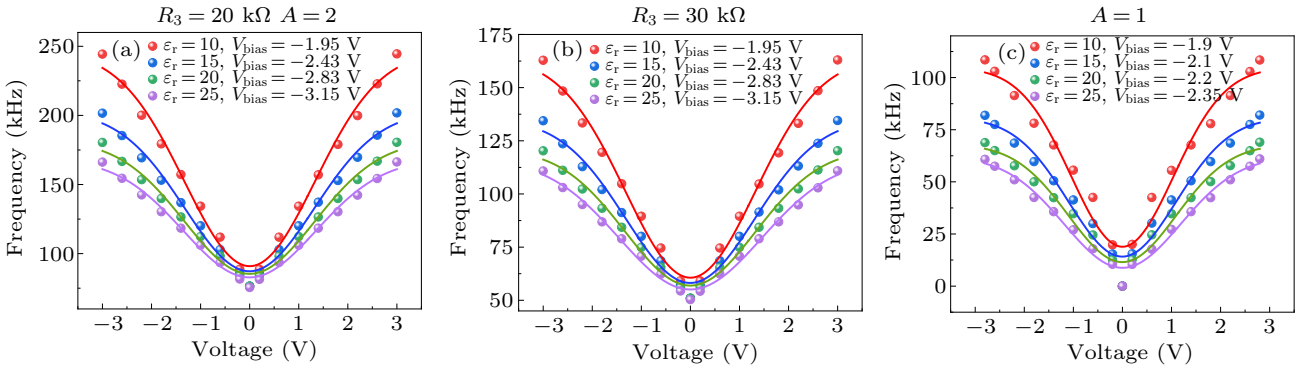

Fig. 7. Frequency characteristic curves of the same output range obtained by changing the circuit parameters. Here, TS memristor models with different dielectric constants are used to modify the response characteristics.

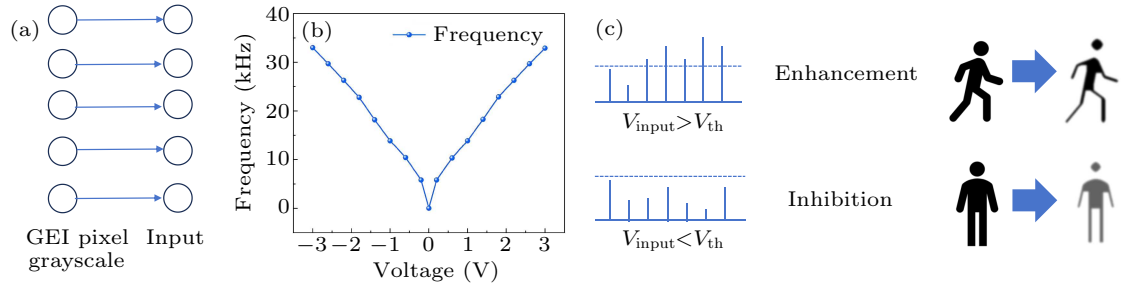

Fig. 8. Processing flow of the gait recognition algorithm: (a) schematic diagram of the mapping process, (b) V–F relationship of the IRBN circuit, (c) schematic diagram of the enhancement and suppression process. Here V_{th} is the threshold voltage defined in the text; top: the threshold voltage (motion feature) indicates enhancement; bottom: the threshold voltage (static feature) indicates inhibition.

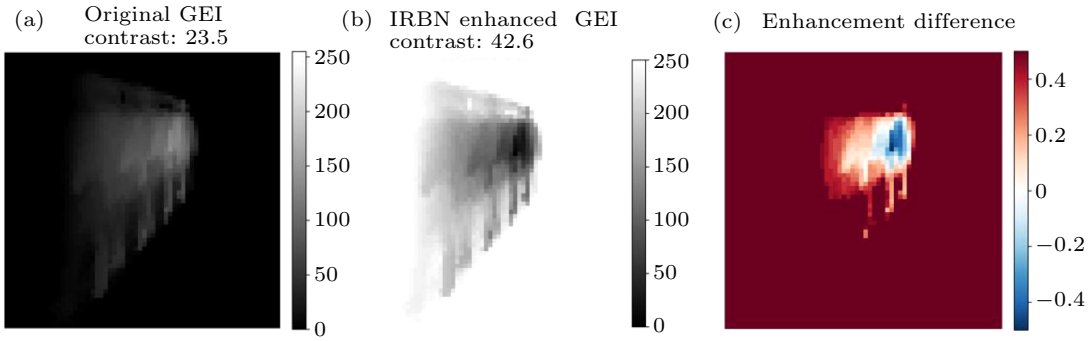

Fig. 9. (a) Original gait energy maps. (b) Gait energy map processed by the IRBN method. Overall background grayscale is elevated, while brightness in human contour regions is preserved or further enhanced, with markedly increased contrast. (c) Results after IRBN method enhancement.

Here, the GEI recognition task is implemented with the CASIA-B-silh. This dataset contains silhouette sequences of 124 identities under different walking conditions. In specific experiments, 50 GEI samples of 64×64 pixels were selected and preprocessed using the IRBN algorithm and 7 traditional image processing methods, with performance evaluated through 3 quantitative metrics. Its performance was evaluated using three quantitative metrics: the structural similarity index measure (SSIM) for gauging image similarity, contrast enhancement for amplifying grey-scale differences between foreground and background, and edge retention. The traditional methods covered different types including linear filtering (Gaussian, bilateral[24]), grayscale transformation (histogram equalization, CLAHE[25]), and edge enhancement (sharpening, morphological operations[26]).

By pixel-wise averaging all digitized silhouette frames over an entire gait cycle, the 'raw GEI map' is shown in Fig. 9(a). The presence of high-grayscale value regions indicates that the human contours representing motion features are enhanced in most frames. Conversely, low-grayscale value regions indicate background areas where motion features are not prominent. The contrast value (standard deviation) calculated using a 255-level grayscale range shows that the contrast value of the original GEI map is 23.5, indicating that the original image is overall dark and lacks tonal depth. Following IRBN preprocessing, as shown in Fig. 9(b), the brightness distribution of the original image is remapped and the background is balanced: background grayscale levels are elevated, human contour edges are preserved, overall contrast is significantly enhanced, and details become more discernible. As shown in Fig. 9(c), the difference map shows that IRBN enhancement keeps the background unchanged, darkens certain internal body regions (blue), and brightens body contours (red), thereby improving the separation between the human figure and background.

Simulation results reveal the IRBN method's significant advantage in edge retention. As shown in Fig. 10, the IRBN method achieved 9.466 on the edge preservation index, the highest value among all methods. This significant advantage directly stems from IRBN's non-monotonic V–F characteristics. Specifically, when the input voltage lies within the range of -1 V to 1 V, the output frequency is low, forming a 'near-suppression'. Whereas, when input voltage exceeds -1 V or 1 V, output frequency is high, achieving 'far-enhancement'. When applied to grayscale image processing, this response mechanism simultaneously suppresses weak signals (background noise) and amplifies strong signals (moving contours). The edge preservation index (EPI) is a commonly used objective evaluation metric in the fields of image denoising and image enhancement. It measures the ability of a processed image to retain the edge information of the original image while removing noise. The formula for its calculation is as follows:

$$\mathrm{EPI} = \frac{\sum_{i,j} \left|\nabla \hat{I}(i,j)\right|}{\sum_{i,j} \left|\nabla I(i,j)\right|}, \tag{2}$$

where $I(i,j)$ denotes the original image; $\hat{I}(i,j)$ denotes the processed image, such as one that has undergone denoising or enhancement; $\nabla I(i,j)$ is defined as the gradient of the original image at pixel position (i,j), typically computed via first-order differentiation in the horizontal or vertical direction; the symbol $\hat{I}(i,j)$ denotes the gradient of the processed image at the corresponding pixel, with the summation traversing all pixels in the image.

Concurrently, the IRBN achieves a contrast enhancement factor of 4.088, indicating its effective enhancement of foreground–background distinction. Secondly, the relatively low SSIM value (0.214) reflects the IRBN transformation's significant alteration of the original grey-level distribution, demonstrating the characteristics of its selective enhancement mechanism. This process of amplification and suppression precisely corresponds to edge grey-level differences, thereby ensuring complete edge sharpness preservation. By contrast, linear filtering (Gaussian, bilateral) reduces noise but inevitably blurs edges due to the weighted averaging of the convolution kernel. Grey-scale transformations (histogram equalization, CLAHE) merely stretch the dynamic range while introducing non-linear distortion to edge signals.

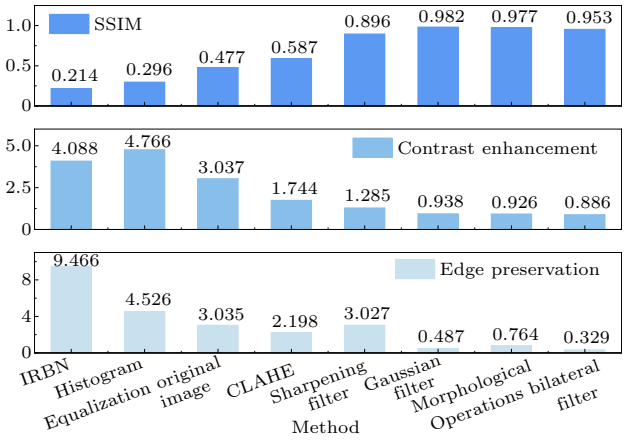

Fig. 10. Simulation results for gait recognition. Three metrics (contrast enhancement, structural similarity index, and edge reservation) are selected to measure the performance of the IRBN method.

Furthermore, the simulation results for rank-1 accuracy using the IRBN and ReLU methods are presented in Fig. 11. This metric measures the proportion of times the model correctly places the identity at the top of the retrieval list, serving as the most commonly employed performance evaluation criterion for gait recognition. The IRBN method achieved a rank-1 accuracy of 96.36% on the CASIA-B-silh dataset, representing a 5.44% improvement over the ReLU method (90.92%). Furthermore, the IRBN method converged more rapidly and stably, reaching its peak accuracy after only 39 epochs. This fully validates that IRBN can significantly enhance motion detection capabilities.

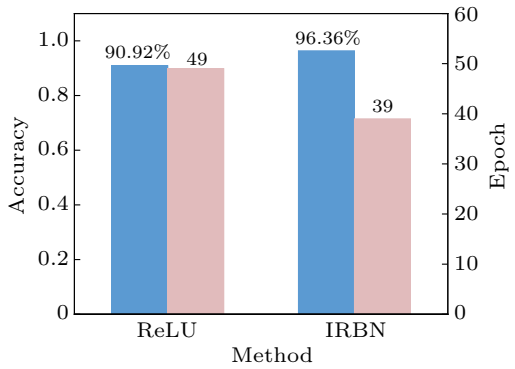

Fig. 11. Comparison of rank-1 accuracy between IRBN and ReLU methods on the CASIA-B-silh dataset.

5. Conclusion

In this work, we successfully developed a memristor-based inverse radial basis neuron (IRBN) circuit for biomimetic motion vision detection. The proposed IRBN circuit exhibits unique "near-suppression far-enhancement" characteristics that naturally match the visual mismatch negativity (vMMN) phenomenon in biological visual systems. The V–F response can be tuned by adjusting the memristor's dielectric constant and circuit parameters. In GEI recognition applications, the IRBN-based preprocessing algorithm achieved an edge preservation index of 9.466, outperforming traditional methods by 2–30 times, validating its superiority in motion feature detection. This work successfully maps memristor device characteristics into visual processing algorithms and provides a new implementation approach for biomimetic motion vision detection.

Acknowledgements

Project supported by the National Natural Science Foundation of China (Grant Nos. 62304001 and 62274002), the Anhui Provincial Natural Science Foundation (Grant Nos. 2308085QF213 and 2408085QF211), and the Natural Science Research Project of Anhui Educational Committee (Grant No. 2023AH050072).

References

[1] Tan H and van Dijken S 2023 *Nat. Commun.* **14** 2169
[2] De Fazio R, Mastronardi V M and De Vittorio 2023 *Sensors* **23** 1856
[3] Peer Mohamed Appa M A Y, Vanitha V, Rishi P, Sagar S and Paul M A 2025 *Sci. Rep.* **15** 30957
[4] Garcia-Duarte J, Mishnayot Y, Tamashiro A S, Lawrence J R and Harke J T 2024 *Sci. Rep.* **14** 7579
[5] Arzehgar A, Seyedhasani S N, Ahmadi F B, Bagheri Baravati F, Sadeghi Hesar A, Kachooei A R and Aalaei S 2025 *BMC Sports Sci. Med. Rehabil.* **17** 15
[6] Hillis J M, Ernst M O and Banks M S 2002 *Science* **298** 1627
[7] Zhu B, Wang H, Liu Y Q, Qi D, Liu Z Y, Wang H, Yu J C, Sherburne M, Wang Z H and Chen X D 2016 *Adv. Mater.* **28** 1559
[8] Kumar D, Li H, Das U K, Syed A M and El-Atab N 2023 *Adv. Mater.* **35** 2300446
[9] Kumar D, Joharji L, Li H, Rezk A, Nayfeh A and El-Atab N 2023 *Light Sci. Appl.* **12** 109
[10] chmitt C, Klingenhoefer S and Bremmer F 2018 *Sci. Rep.* **8** 13598
[11] Guo W, Huang H, Feng Z, Zou J, Lin Z and Xu Z 2025 *IEEE Electron Dev. Lett.* **46** 1425
[12] Li X, Feng Z, Zou J, Wang X, Hu G, Wang F, Ding C, Zhu Y, Yang F, Wu Z and Dai Y 2022 *J. Appl. Phys.* **132** 064904
[13] Wang J, Lu Z, Xing X, Li X, Wang Y, Chen M, Pang G, Qian F, Zhou Y and Han S 2020 *Adv. Funct. Mater.* **30** 1909114
[14] Dai Y, Zou J, Feng Z, Li X, Wang X, Hu G, Zhu Y and Wu Z 2022 *Semicond. Sci. Technol.* **37** 095001
[15] Dang B, Zhang T, Wu X, Liu K, Huang R and Yang Y 2024 *Nat. Electron.* **7** 991
[16] Feng Z, Zou J, Guo W, Fang X, Chen T, Ma X, Yu R, Tan S, Hu Y, Wang Z, Xu Z, Zhu Y, Dai Y and Wu Z 2025 *IEEE Trans. Circuits Syst. II* **71** 4051
[17] Pu L, Li Y and Gao P 2022 *Sci. Rep.* **12** 9563
[18] Zhu J, Zhang X, Wang R, Wang M, Chen P, Cheng L, Wu Z, Wang Y, Liu Q and Liu M 2022 *Adv. Mater.* **34** 2200481
[19] Wu Z, Zhang C, Zou J, Peng C and Wu X 2023 *IEEE Trans. Circuits Syst. II* **70** 1034
[20] Lin C H, Tsai J S and Chiu C T 2010 *IEEE Trans. Image Process.* **19** 2307
[21] Wu Z, Li W, Zou J, Feng Z, Chen T, Fang X, Li X, Zhu Y, Xu Z and Dai Y 2024 *IEEE Trans. Circuits Syst. II* **71** 1446
[22] Wu Z, Hu Y, Feng Z, Zou J, Guo W, Lu J, Shi T, Tan S, Wang Z, Yu R, Zhu Y, Xu Z and Dai Y 2024 *Appl. Phys. Lett.* **124** 233505
[23] Giesselmann M and Roy V 2018 *Proc. IEEE IPMHVC* **3** 162
[24] Kalsoom A, Iftikhar M A, Ali A, Shah Z, Balakrishnan S and Ali H 2025 *Sci. Rep.* **15** 21881
[25] Narla V L, Suresh G, Rao C S, Al Awadh M and Hasan N 2024 *Sci. Rep.* **14** 27588
[26] Maragos P 1989 *IEEE Trans. Pattern Anal. Mach. Intell.* **11** 701